# **Effect of Presetting and Deep Rolling on Creep of Torsion Spring Bars**

Vinko Močilnik − Nenad Gubeljak ⊠ − Jožef Predan University in Maribor, Faculty of Mechanical Engineering, Slovenia ⊠ nenad.gubeljak@um.si

**Abstract** This study investigates the creep behavior of torsion spring bars by combining experimental testing and numerical modeling. Experimental investigations were performed on torsional specimens subjected to different presetting levels and deep rolling surface treatments, showing different effects on stress relaxation at a constant torsion angle. Finite element method (FEM) simulations incorporating elasto-visco-plastic material behavior successfully reproduced the time-dependent deformation observed experimentally. Material parameters for the FEM model were derived from experimental data. The findings show that a two-stage presetting process combined with intermediate deep rolling results in higher residual compressive stresses in the surface layers compared to a single-stage presetting process. Although this method aims to mitigate creep under constant loading conditions, its effectiveness is limited. A reduction in creep strains is only observed up to a presetting level of approximately 4.3 %; above this threshold, creep strains increase significantly and loading capacity decreases.

Keywords creep; torsion bar; FEM analyzis; presetting, deep rolling; torque, twist angle

#### **Highlights**

- The material parameters for the FEM model were derived from experimental creep data.
- The experimental measured tensile creep data can be used to numerical simulation of creep torque.
- The optimal life is within a narrow range of prestressing and rolling-induced residual stresses.

## 1 INTRODUCTION

Torsion bars are commonly used in suspension systems to absorb road surface irregularities and shocks in both wheeled and tracked vehicles. To increase the elastic (linear) operating range, torsion bars are strain-hardened—preset in the direction of subsequent torsional loading—to introduce compressive stresses into the surface layers. An additional component of compressive stress is introduced into the surface layers through the deep rolling process.

Previous investigation shows that the stress state of a torsion bar under torsional loading by analyzing the effects of various distributions of residual and applied stresses, using the Drucker-Prager criterion to assess the actual stress condition [1]. The findings indicate that the fatigue limit is maintained as long as the combined principal stresses remain within the safe zone. However, increasing compressive residual stresses near the surface can alter their distribution in depth and potentially shift the principal stress amplitude outside the safe zone as defined by the Drucker-Prager criterion.

In [2], a dynamic explicit simulation was used to analyze the residual stresses induced by the deep rolling process on a high-strength steel torsion bar. A three-dimensional simulation of a representative section effectively replicated the residual stress profile generated during deep rolling. The final stress magnitude is significantly influenced by the process input parameters. Additionally, the depth distribution of these residual stresses is strongly dependent on the dimensions of the extracted model. Therefore, it is crucial to carefully choose modeling assumptions and simplifications, as they directly affect the accuracy of the simulation results. The finite element model developed for the deep rolling process provides a solid foundation for future numerical studies.

It was an established model for fatigue lifetime prediction where the torsion-bar springs show different fatigue behavior depending on the applied elastic-plastic preset torque [3]. The study analyzed how presetting the twist angle affects fatigue life under various strain conditions. Presetting causes plastic deformation at the outer surface, while the core remains elastic, leading to compressive residual stresses. Increasing the preset torque allows for a larger twist angle but reduces fatigue life. Experiments showed that fatigue life strongly depends on the ratio between preset load and fatigue loading range.

Perenda et al. [4] highlighted the significant influence of residual stresses on the fatigue life and load capacity of torsion bars. Deep rolling induces compressive stresses in the subsurface, which suppress crack formation. Presetting overstrains and hardens the bar, increasing residual shear stresses and material yield strength, thereby enhancing load capacity. The study simulated various sequences of deep rolling and presetting using mapping and FE analyzis on a cutout model, with results validated by measured residual stresses.

Residual stresses were measured on the surface of a round specimen during torsional presetting, specifically in the principal directions of +45° (compressive) and -45° (tensile) [5]. These stresses follow a linear distribution in the elastic range and become nonlinear once the material exceeds its elastic limit. Initial residual stresses were introduced by surface cold rolling, which plastically deforms a shallow surface layer. This process induces anisotropic strain due to material flow in both axial and circumferential directions, resulting in a helical lattice structure and differing stress values in each direction. Torsional characteristics derived from converted tensile data ( $\sigma$ - $\varepsilon$  to  $\tau$ - $\gamma$ ) showed slight deviations from direct torsion test results. Residual stresses were analytically calculated based on both datasets and compared. Additionally, FEM simulations using ABAQUS Release 2025, based on tensile properties, confirmed the analytical results.

Blum et al. [6] were compared experimental results on creep kinetics and microstructural evolution with the predictions of a simple, spatially homogeneous plastic deformation model. The model

DOI: 10.5545/sv-jme.2025.1407

describes the development of the dislocation structure as well as the creep kinetics.

Kolev et al. [7] were introduced a new expression for the creep law aiming to study in detail the behavior of simple structures using a generalized creep law with separable variables. The new expression, based on experimental data, combines the primary, secondary, and tertiary regions of the creep curve. The relaxation functions for bending and torsion depend solely on the maximum stress in the cross-section that occurs on the outer surface.

In [8], the main objective is to derive exact closed-form expressions for torsional and flexural creep in isotropic materials, based on generally accepted constitutive laws. The Norton-Bailey, Prandtl-Garofalo, and Naumenko-Altenbach-Gorash laws permit a closed-form solution. A partial generalization of the Norton-Bailey law is also solved in closed form. Stress relaxation was studied for structural elements subjected to torsional and flexural loads. The structures examined—such as a beam in bending, a bar in torsion, and a coil spring—demonstrate the fundamental characteristics of nonlinear creep. Closed-form solutions, using common creep models, provide a deeper understanding of the inherent effects in structural elements and support the design process.

Several authors have investigated biaxial loading with torsion and axial force on cylindrical specimens.

Šeruga at al. [9] developed a software tool for predicting creep damage in thermo-mechanically loaded components. It enables master curve determination using time-temperature parameters and calculate creep damage based on Robinson's rule and simple time integration. The software also allows separate evaluation of fatigue and creep damage. The article presents commonly used time-temperature parameters, a fast and user-friendly method for master curve generation, and an example of creep damage calculation using real data with a simple temperature-stress history [9].

Makabe and Socie [10] analyzed the fatigue crack growth in precracked torsion specimens and find that friction of the crack surfaces prevented shear mode crack growth. Yang and Kuang [11] examined the crack paths and growth rates of S45 steel specimens under various combinations of torsional and constant axial loads. They reported that the crack propagation angle was approximately 45° for different load amplitudes. Static tension combined with axial force and cyclic torsion accelerated crack growth and reduced service life, while compressive axial force combined with torsion significantly increased service life without affecting the crack propagation angle. They also found that the crack propagation direction depended on the alternating stress amplitude and was independent of the mean stress.

Tanaka et al. [12] tested hollow lead-free solder samples under torsional and combined torsional and compressive axial loads. They found that the crack initially propagated in the direction of maximum shear stress and later in the direction perpendicular to the maximum principal stress. Numerous microcracks formed between individual phases within the material's lattice, which later coalesced into a single crack.

Grigoriev at al. [13] investigated that grinding kinematics play a key role in the efficiency of creep-feed grinding. Paper examines non-traditional parameters—such as removal area, force ratios, and depth-to-diameter ratio—through three case studies on turbine blades, gears, and broaches using low-speed vitrified alumina wheels. Though experimental details are omitted, practical guidelines for improving productivity and quality are provided.

Nagode and Fajdiga [14] investigate that the isothermal strain-life method, commonly used for low-cycle fatigue, is fast and typically based on elastic finite element analyzis. Adapted for variable temperatures using a Prandtl-type operator, it assumes stabilized hysteresis loops and neglects creep. Reversal point filtering is examined, and the method is compared with thermo-mechanical

fatigue tests and the Skelton model. In [15], the authors use the same approach when considering creep in the case of a press fit load capacity study.

This article investigates the creep behavior of torsion bars for two levels of presetting, specifically 4.3 % and 5.1 % surface shear strain. For each case, creep was comparatively evaluated for both manufacturing technologies, Technology A and Technology B. The creep of the torsion bars was assessed through experimental testing and FEM numerical simulation.

#### **2 METHODS AND MATERIALS**

The final geometry of the torsion bar is produced using a suitable material and appropriate mechanical properties. The manufacturing process involves rolling, hardening, tempering, and mechanical cutting. This is followed by deep rolling, which smooths the surface and introduces significant compressive residual stresses into the surface layers of the torsion bar. In addition to inducing compressive residual stresses, deep rolling also improves corrosion resistance and surface wear characteristics.

After deep rolling, the process of increasing the elastic operating range—known as presetting—is carried out. During presetting, the torsion bar is strain-hardened by controlled multiple transitions into the plastic region of the material under torsional loading [4]. This establishes a new, higher elastic limit. Upon unloading, residual torsional deformation remains, along with significant residual stresses. In the surface layers, these residual stresses are compressive, while in the core of the torsion bar, they are tensile. The compressive surface stresses enhance the cyclic fatigue strength, which is critical since torsion bars are designed for a defined service life with a limited number of load cycles. The torsion bar manufactured in this way is intended to be loaded with a unidirectional torsional moment, in the same direction as the presetting.

The introduction of residual stresses through deep rolling enhances the cyclic endurance of the torsion bar, while the presetting process tends to reduce its service life. It has been shown that performing presetting after deep rolling reduces the compressive residual stresses at the surface [4,5]. The number of loading cycles until failure depends on the degree of presetting as well as the load magnitude during testing or in actual use of the torsion bar [3]. In addition to reducing service life, increased presetting also leads to larger creep or yielding strains of the torsion bar under constant load.

To stabilize creep, a slightly modified manufacturing process has been adopted in practice. It has been shown that maintaining sufficiently high compressive stresses on the surface during the production of the torsion bar is crucial. This modified process involves partial presetting before deep rolling, followed by final presetting after deep rolling. This approach helps preserve a relatively high level of compressive residual stresses on the surface of the torsion bar [4] and reduces creep.

The first process, referred to as Technology A, consists of deep rolling followed by presetting the torsion bar into the plastic region. The second process, referred to as Technology B, involves partial presetting into the plastic region, then deep rolling, and finally final presetting [2].

### 2.1 Material Properties and Manufacturing Technology

Torsion bars were manufactured from high-strength, fine-grain spring steel grade 150VCN (according to EN 10027-1:2016 [16] 50CrV4, W. Nr. 1.8159). Figure 1 shows tensile tests results. The chemical composition (in weight %) and mechanical properties are listed in Tables 1 and 2, respectively [3]. Material has high yield strength Re

and ultimate tensile strength (UTS) Rm more than 2000 MPa. The material used was hot-rolled, forged, and soft annealed during the manufacturing process. The final shape and properties were achieved through the following mechanical processes: programmed turning, milling, and polishing.

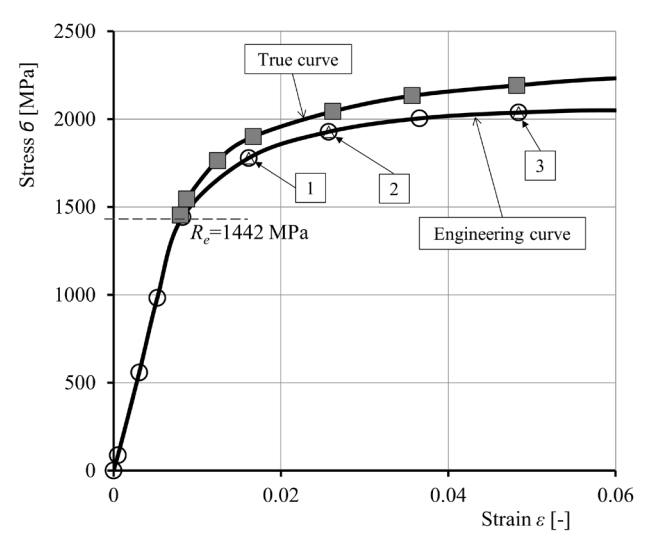


Fig. 1. True and engineering curves

The torsion specimen shown in Fig. 2b had a diameter of d = 10 mm, with a root-split section and a calculated effective length of l = 250 mm. The surface of the bar was polished to a roughness of Ra = 0.2 µm. The torsion bars were hardened using a dedicated process to achieve a target hardness of  $54 \pm 1$  HRC. Surface rolling and presetting were carried out as described in [4].

Table 1. Chemical composition in weight % of the used material, as specified in [4]

	С	Si	Mn	Ni	Cr	Мо	٧	Cu	S	Р
Actual val.	0.44	0.28	0.56	1.41	0.87	0.26	0.11	0.12	0.002	0.009
Min.	0.42	0.17	0.5	1.3	0.8	0.2	0.1	0	0	0
Max.	0.5	0.37	0.8	1.8	1.1	0.3	0.18	0.25	0.002	0.009

Figure 1 presents the engineering and true stress-strain curves for the material in its tempered condition. The engineering curve was obtained through tensile testing at ambient temperature, while the true curve was derived by calculation. The yield strength was determined using the following expression:

$$\sigma_f = \sigma(1 + \varepsilon),\tag{1}$$

and logarithmic strain:

$$\varepsilon' = \ln(1 + \varepsilon),\tag{2}$$

where  $\sigma_f$  is the true stress [MPa],  $\sigma$  engineering stress [MPa],  $\varepsilon$  engineering strain [-], and  $\varepsilon'$  true strain [-].

Table 2. Average mechanical properties of the torsion bar for different loading ratio  $R = \sigma_{min} / \sigma_{max}$ 

Yield strength,	UTS.	Poisson.	Torsion elastic	Shear modulus.	Modulus.	Tensile fatique limit	Tensile fatique limit	Torsion fatique limit
Re [MPa]	Rm [MPa]	v [-]	limit, $\tau_e$ [MPa]	G [GPa]	$E\left[GPa\right]^{'}$	R = 0, [MPa]	R = -1, [MPa]	R = -1, [MPa]
1442	2010	0.3	800	80	193	1200	800	520

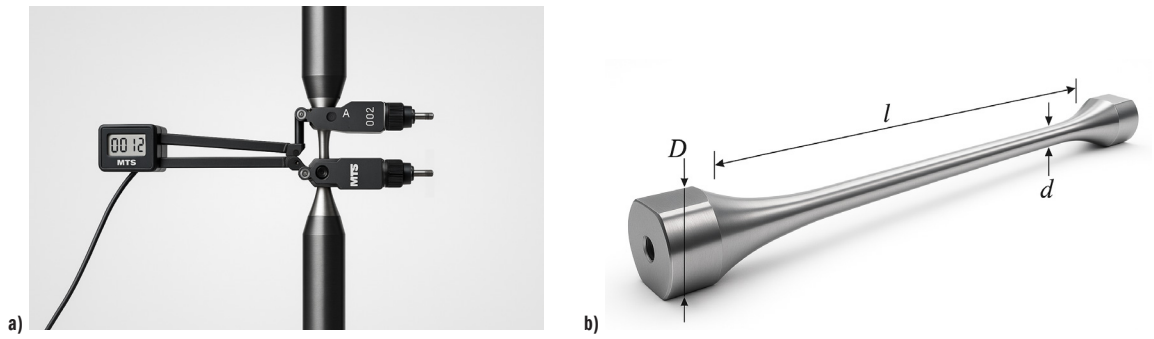


Fig. 2. Setup for creep tension testing with; a) elongation measurement, and b) torsion bar specimen

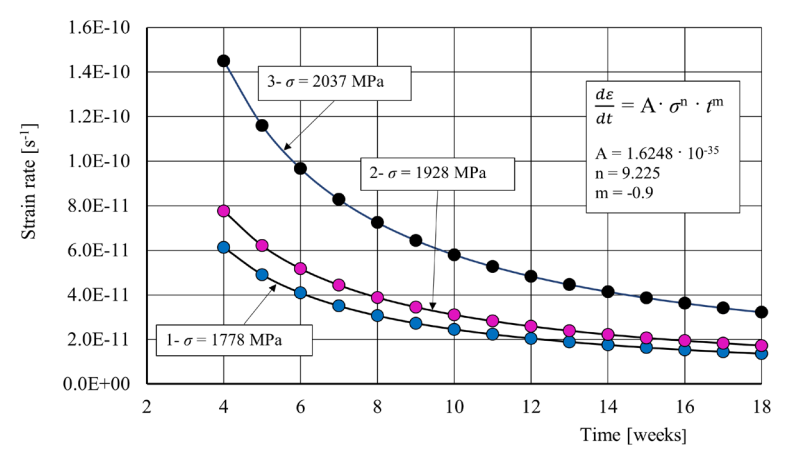


Fig. 3. Time dependent properties of the used material

A creep test under constant stress was performed on the material. Figure 2a shows the setup for creep tension testing with elongation measurement on the INSTRON 1255 servo-hydraulic testing machine. In Figure 1, points 1, 2, and 3 indicate the locations where stress relaxation was measured. Three tensile specimens were loaded to specific stress levels and then held under constant plastic strain. Plastic strain was measured using an extensometer, and the moment when the target stress was reached was defined as time zero. Figure 3 illustrates the dependence of creep strain rate on time under constant stress. The three stress levels considered were 1778 MPa, 1928 MPa, and 2037 MPa. The parameters *A*, *n*, and *m* were experimentally determined for use in ABAQUS finite element simulations.

$$\dot{\varepsilon} = A\sigma^n t^m,\tag{3}$$

where  $\dot{\varepsilon}$  is uniaxial equivalent creep strain rate;  $\sigma$  uniaxial equivalent deviatoric stress, and A, n, m are constants determined experimentally at room temperature.

## 2.2 Torsion Specimen Preparation

The specimens were manufactured using the same technological process as that used for standard torsion bar production. The final shape and properties were achieved through programmed turning, milling, and polishing of the torsion bar body to a surface roughness of  $0.2 \ \mu m$ . The geometry of the specimen is shown in Fig. 2b.

In Figure 4 provides a recommended presetting level for achieving optimal service life during torsion bar production, depending on the magnitude of the load applied during testing or actual use [3]. In the diagram, the presetting shear strain ( $\gamma_{ps}$ ) and the applied shear strain ( $\gamma_{app}$ ) represent the surface strain on the torsion bar. The upper curve denotes the elastic limit, while the lower curve corresponds to the high-cycle fatigue limit. The area between these two curves represents the optimal service life range for torsion bars. Red lines within this area are isolines indicating constant service life.

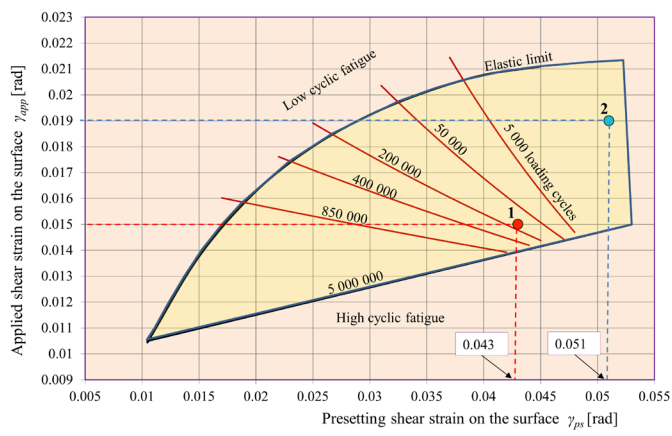


Fig. 4. Lifetime optimum zone of the torsion bar [3]

The service life of a torsion bar is influenced by the degree of presetting and the intensity of the cyclic torsional loading during operation. Additionally, presetting introduces creep, which results in vehicle settling under a constant load. In practice, a presetting surface shear strain of  $\gamma_{ps}$  = 4.3 % is generally considered an acceptable upper limit, beyond which both service life and creep behavior remain within acceptable bounds. However, in some cases, presetting beyond 4.3 % may be required, though this leads to a significant increase in creep.

Experimental results have shown that, in terms of minimizing creep, it is more favorable to perform presetting in two stages with intermediate deep rolling. As outlined in the introduction, two torsion

bar preparation methods are considered in this study: Technology A, involving a single presetting after deep rolling, and Technology B, which uses a two-step presetting process with intermediate deep rolling.

In the diagram shown in Fig. 4, points 1 and 2 indicate the preparation and testing parameters of the torsional specimens. For both points, the two technologies, Technology A and Technology B were applied. The diagram reflects the results of long-term torsional testing, thereby indirectly accounting for creep behavior as well.

Table 3 presents the preparation parameters of the specimens used in the torsional creep tests. The symbols in the table represent:  $g_{ps}$  [%] shear strain on the surface of the torsion specimen at presetting,  $f_{ps}$  [°] twist angle of the torsion specimen at presetting,  $g_{app}$  [%] shear strain on the surface of the torsion specimen at application or at testing,  $f_{app}$  [°] twist angle of the torsion specimen at application or testing, and  $f_{0}$  [Nm] initial torque.

Table 3. Preparation of torsion specimens (DR - Deep rolling; P - Presetting)

Point	$g_{ps}$ [%]	$f_{ps}$ [°]	g <sub>app</sub> [%]	$f_{app}$ [°]	Initial torque $T_0$ [Nm]	Technology
1	4.3	123	1.5	43	206	A (DR-P)
1	4.3	123	1.5	43	206	B (P-DR-P)
2	5.1	146	1.9	54.4	237	A (DR-P)
2	5.1	146	1.9	54.4	237	B (P-DR-P)

Figure 5 illustrates the preparation parameters for torsional specimens used in creep testing. The points labeled 1-A, 1-B, 2-A, and 2-B correspond to the positions in the diagram in Fig. 4, representing the respective technological preparation methods A and B. Each of these marked points indicates the starting point for measuring the time-dependent torque during creep at a constant twist angle.

After the torsional specimens were prepared through deep rolling and presetting, they were loaded to a twist angle of either 43° (initial torque  $T_0 = 206$  Nm) or 54° ( $T_0 = 237$  Nm), respectively. The change in torque over time due to creep was then measured and recorded.

## 2.3 Torsion Test Method

During the presetting phase, the torsion bar must be deliberately overloaded in a controlled manner into the plastic region, while measuring both torque and twist angle. A dedicated torsional loading device was designed for this purpose, as shown in Fig. 6.

On one end of the tested torsion specimen, a clamping sleeve is connected to a WATT DRIVE gear unit, type FUA 65A 101LA4 BR20 FL, 3 kW, 10 min<sup>-1</sup>. The gear is driven by an electric motor, with speed regulated by a V2500 frequency control unit from the same manufacturer. On the opposite side of the gear's hollow shaft, a SIMODRIVE incremental encoder (Siemens, Germany) is installed, offering an angular measurement resolution of 5000 pulses per revolution.

Torque is measured using a DF-30 (500 Nm) torque sensor from Lorenz Messtechnik. For data acquisition and visualization, the torque sensor and incremental encoder are integrated into a measurement chain consisting of Spider-8 universal PC measuring electronics and the Catman EASY software, both from HBM.

#### 2.4 FEM Simulation

The finite element analyzis of the stress-strain state was conducted using the SIMULIA Abaqus 2025 software suite [17]. A comprehensive three-dimensional simulation of a torsion spring was performed, employing a single-layer discretization of finite elements

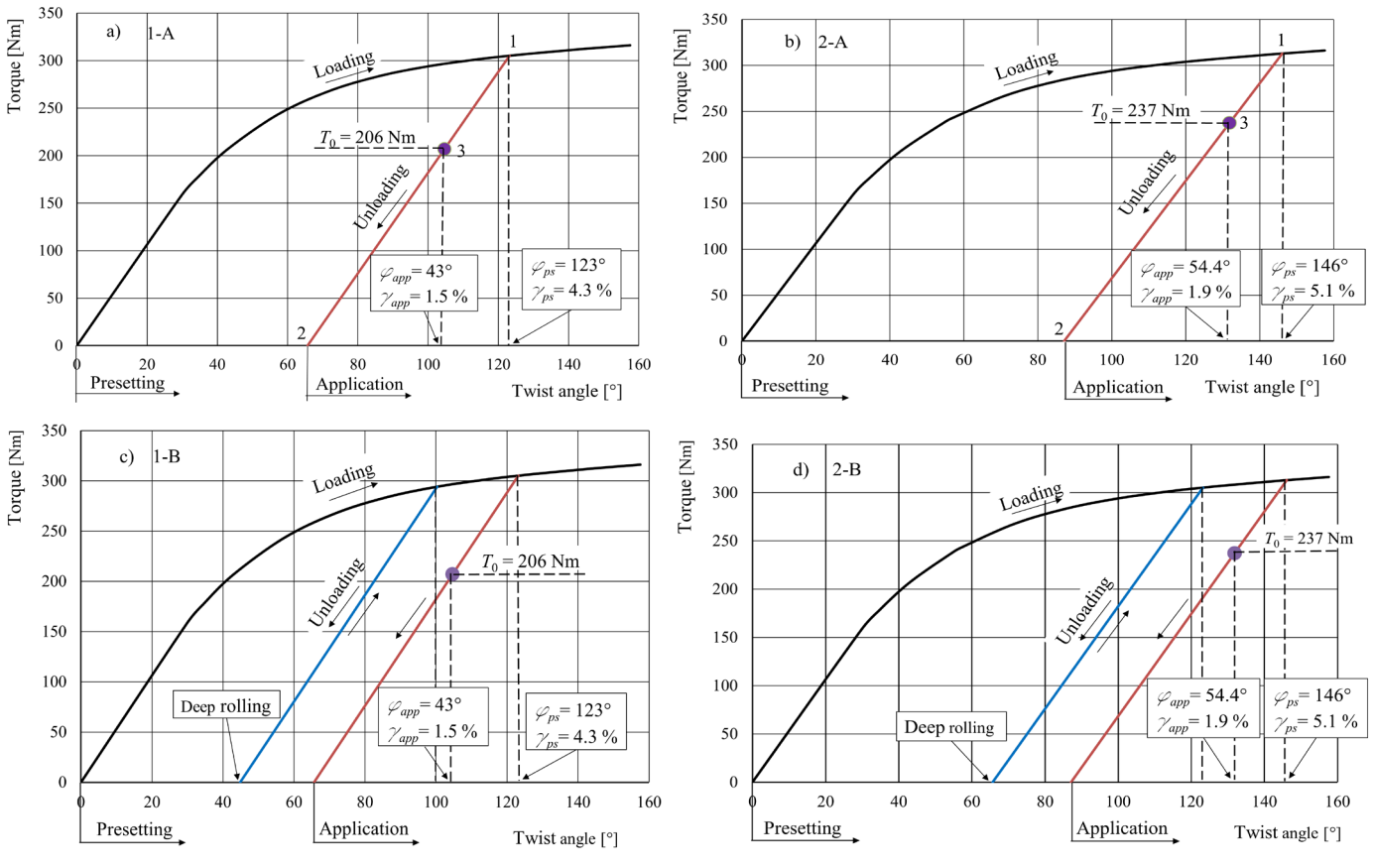


Fig. 5. Preparation of torsion specimens with presetting

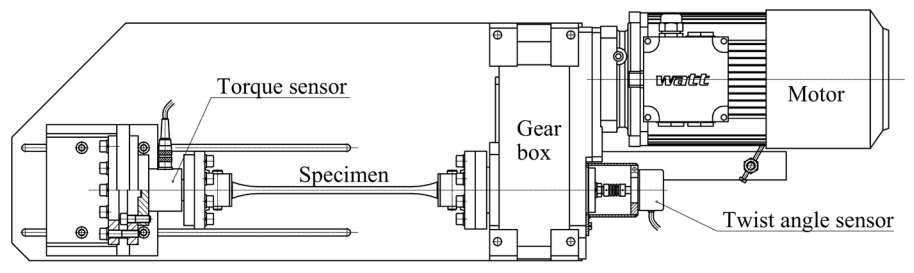


Fig. 6. Presetting device [3]

along the spring's axial direction. Eight-node brick elements (C3D8) were utilized throughout the model. Appropriate boundary conditions were imposed on the free end surfaces of the thin, singlelayer configuration to ensure well-posedness of the problem and to enable the accurate determination of stress-strain responses under torsional loading. This modeling strategy significantly reduced the computational complexity and numerical size of the model, thereby enabling rapid and efficient numerical simulations, while still capturing the complete stress-strain field that would be observed in a full-length spring model. The material analyzed in this study is isotropic and homogeneous spring steel. Therefore, it was essential to determine the key material parameters through experimental testing in order to accurately describe its elastic-plastic and additional viscoelastic behavior. Similar approach was applied in the research study [18] where analyzes the evolution patterns of damage parameters concerning sheet metal and corresponding temperatures. Possible applications are described in testing of in special off-road vehicles and their parts [19].

The material behavior was characterized using an elastic-plastic-visco-plastic constitutive model. This allowed for the accurate

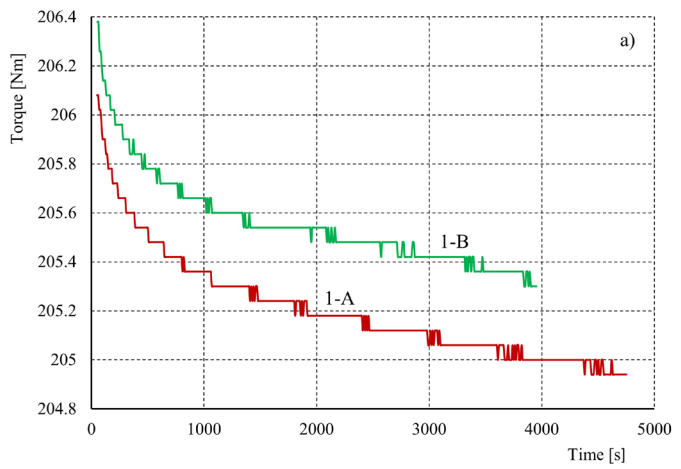
simulation of key physical phenomena, including material yielding, the development of residual stresses due to preloading, and long-term stress relaxation effects attributable to creep. In the linear elastic regime, the material was defined by a Young's modulus of 193 GPa and a Poisson's ratio of 0.3. The yield strength was specified as 1442 MPa, with strain hardening extending to 2010 MPa. Time-dependent material behavior was modelled using a creep formulation that incorporated experimentally determined hardening parameters:  $A = 1.6248 \times 10^{-35}$ , n = 9.47, and m = -0.9. The final simulation employed a total of 47.630 C3D8 elements within the single-layer model, achieving a high-fidelity representation of the stress–strain field in the torsion spring.

#### **3 RESULTS AND DISCUSSIONS**

Figure 7 displays the measured torque values at a constant twist angle as a function of time for all four torsion bar cases. The measured data in the graphs are approximated using an analytical logarithmic function, given by Eq. (4). Table 4 summarizes the constants a and b

for each of the four torsional moment measurements. The analytical function in Eq. (4) describes the experimental results with a mean coefficient of determination of  $R^2 = 0.98$ .

Sudden drops observed in the torque measurements due to creep are attributed to the fact that the measured decrease in torque is smaller than the resolution of the measurement system.



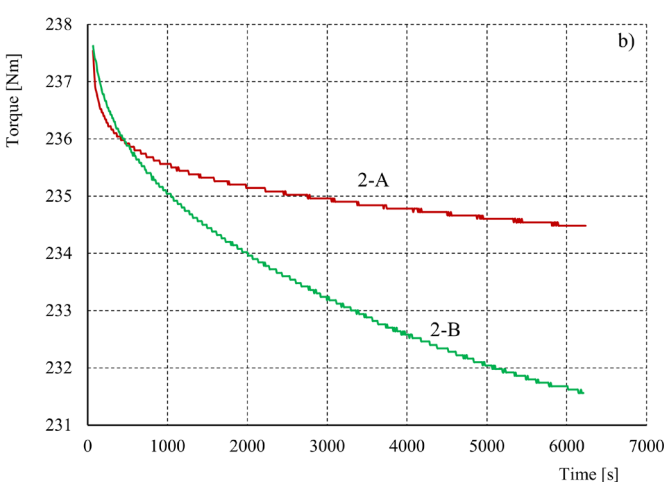


Fig. 7. Time dependent torque measured at a constant twist angle; a) 1-A and 1-B, and b) 2-A and 2-B

Table 4. Constants a and b for Eq. (4)

Point	а	b
1-A	-0.24313	216.53131
1-B	-0.21623	207.14633
2-A	-0.56792	239.46698
2-B	-0.56792	245.73548

$$T(t) = a \cdot \ln(t) + b, \tag{4}$$

where T(t) is dependent torque, t time and a, b are constants.

Figure 8 illustrates the relative torque drop over time. The curves represent the predicted torque reduction as a function of the specimen preparation technology, based on Eq. (4). For comparison, the torque drop predicted by FEM simulation is also shown for case 1-A. The most significant creep is observed at point 2 using Technology B, with a torque drop exceeding 7 %. In contrast, much smaller creep is observed at point 1, where Technology B results in less creep than Technology A.

The results of the creep analyzis for the torsion bars are summarized comparatively in Table 5. After 18 weeks of creep testing, the largest relaxation was observed at point 2 for Technology B, despite the fact that Technology B was designed to reduce torsion bar relaxation. Using the diagram in Fig. 4, the service life of a cyclically loaded torsion bar can be estimated as a function of the applied surface shear strain and the surface presetting shear strain. The upper region of the diagram corresponds to low-cycle fatigue, while the lower region corresponds to high-cycle fatigue. Within the hatched area, lines indicate constant service life. By locating the operating point on the diagram—point 1 or 2 in our case—it is possible to estimate the expected service life of the torsion bar.

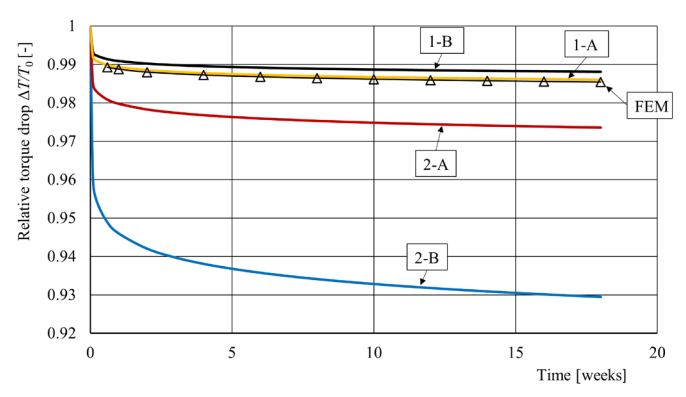


Fig. 8. Prediction of relative time dependent torque drop;  $\Delta T$  is torque drop

Table 5. Relative torque drop in 18 weeks at a constant twist angle and estimated lifetime

Point	Initial torque $T_0$ [Nm]	Relative torque drop in 18 weeks [%]	Estimated lifetime, Fig. 4 [cycles]
1-A	206	1.39	200,000
1-B	206	1.19	200,000
2-A	237	2.64	< 40,000
2-B	237	7.05	< 40,000

A comprehensive three-dimensional simulation of a torsion spring was performed, employing a single-layer discretisation of finite elements along the spring's axial direction, as shown in Fig. 9. Figure 10 presents the results of the FEM analyzis performed to simulate the specimen preparation process, which includes both presetting and creep. Fig. 10a illustrates the residual stresses at point 2 after the presetting step, while Figs. 10b and c depict the applied stresses at point 3, captured before and after the creep process, respectively. The locations of points 2 and 3 are marked in Fig. 5 for reference.

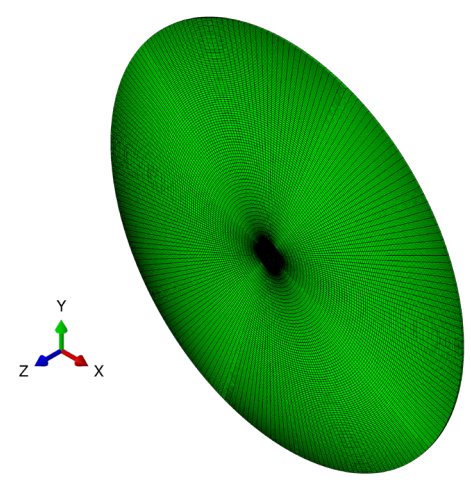


Fig. 9. Finite element model, mesh and interaction constraints

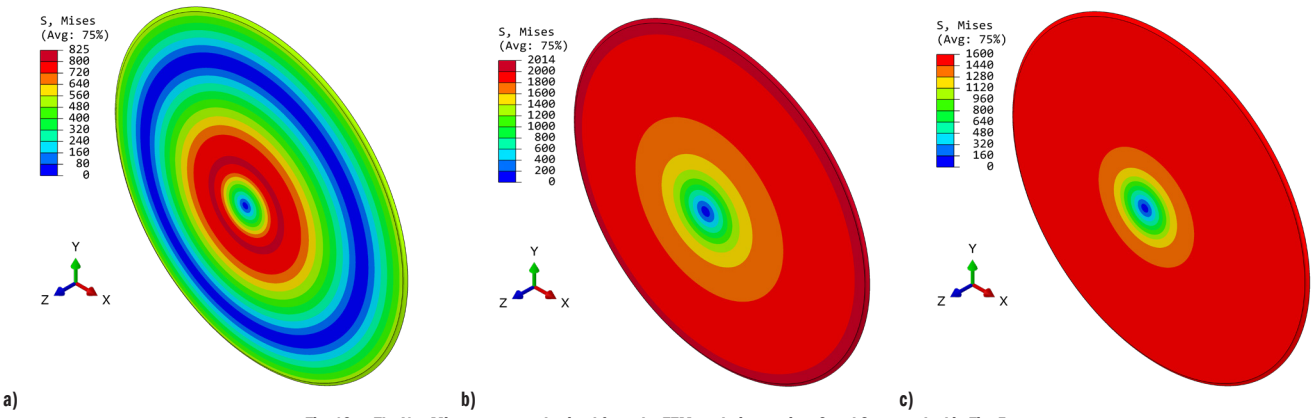


Fig. 10. The Von Mises stresses obtained from the FEM analyzis at points 2 and 3, as marked in Fig. 5, a) residual stresses after presetting at Point 2, b) applied stresses at point 3, and c) aplied stresses at Point 3

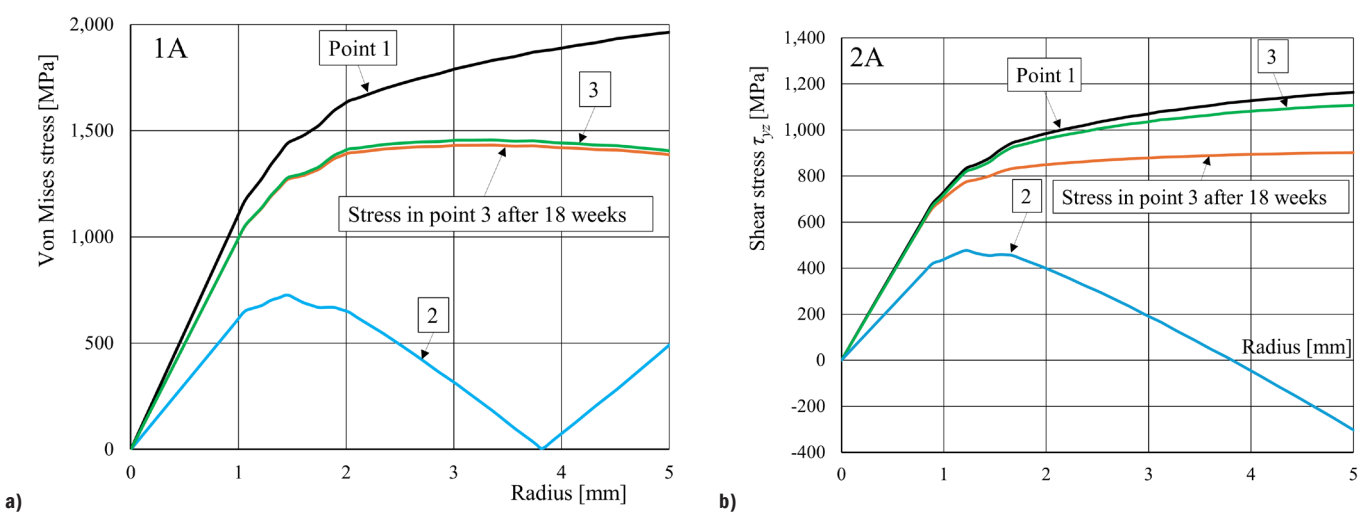


Fig. 11. a) Von Mises, and b) Shear stress distribution across section of torsion bar calculated using FEM analyzis at point 1, point 2 and point 3 from Fig. 5

Figure 11 illustrates the distribution of Von Mises and shear stresses across the cross-section of the torsion bar, as determined by FEM analyzis. Curve 1 represents the stresses introduced during presetting, while Curve 2 shows the residual stresses remaining after unloading. Curve 3 depicts the stresses under the applied load, including the additional creep stresses accumulated over a period of 18 weeks. Measurement points 1, 2, and 3 correspond to the locations identified in Fig. 5.

## 4 CONCLUSIONS

This study investigated the creep of torsion bars subjected to different manufacturing processes involving presetting and deep rolling. Two technological approaches were compared: Technology A (deep rolling followed by presetting) and Technology B (partial presetting, deep rolling and final presetting).

Experimental results showed, that at moderate levels of presetting (4.3 % shear strain), Technology B resulted in lower torque release over time compared to Technology A, confirming the advantage of maintaining high surface compressive stresses via intermediate deep rolling. At higher presetting levels (5.1 % shear strain), creep increased significantly regardless of the process used. However, Technology B resulted in an even higher creep rate than Technology A, likely due to the redistribution of internal stresses caused by excessive plastic deformation.

The FEM numerical simulations accurately captured the timedependent stress relaxation behavior observed in the experiments, demonstrating the capability of the model to reflect real material responses over time. Furthermore, the results validated the application of visco-plastic material models for simulating longterm deformation processes. The simulations also provided strong support for the experimental findings, confirming the reliability and consistency of the observed phenomena.

In conclusion, a balanced presetting rate combined with an optimized deep-rolling sequence can significantly affect the long-term performance and dimensional stability of torsion bars. Excessive presetting should be avoided as it leads to undesirable creep effects that compromise component reliability. Future work should include a more detailed parametric study of the visco-plastic behavior under different temperature and loading conditions, and an analyzis of the interaction between fatigue and creep.

#### **References**

- Močilnik, V., Gubeljak, N., Predan, J. Effect of residual stresses on the fatigue behaviour of torsion bars. Metals 10 1-16 (2020) D0I:10.3390/met10081056.
- [2] Perenda, J., Trajkovski, J., Žerovnik, A., Prebil, I. Residual stresses after deep rolling of a torsion bar made from high strength steel. J Mater Process Technol 218 89-98 (2015) D0I:10.1016/j.jmatprotec.2014.11.042.
- [3] Močilnik, V., Gubeljak, N., Predan, J. Model for fatigue lifetime prediction of torsion bars subjected to plastic Pre-setting. Tech Gazette 18 537-546 (2011).

- [4] Perenda, J., Trajkovski, J., Žerovnik, A., Prebil, I. Modeling and experimental validation of the surface residual stresses induced by deep rolling and Pre-setting of a torsion bar. Int J Mater Form 9 435-448 (2016) D0I:10.1007/s12289-015-1230-2.
- [5] Močilnik, V., Gubeljak, N., Predan, J. Surface residual stresses induced by torsional plastic pre-setting of solid spring bar. Int J Mech Sci 92 269-278 (2015) D0I:10.1016/j.ijmecsci.2015.01.004.
- [6] Blum, W., Eisenlohr, P., Breutinger, F. Understanding Creep-a Review. Metall Mater Trans 33 291-303 (2002) D0I:10.1007/s11661-002-0090-9.
- [7] Kobelev, V. Relaxation and creep in twist and flexure. Multidiscip Model Mater Struct 10 304-327 (2014) D0I:10.1108/MMMS-11-2013-0067.
- [8] Kobelev, V. Some basic solution for nonlinear creep. Int J Solids Struct 51 3372-3381 (2014) D0I:10.1016/j.ijsolstr.2014.05.029.
- [9] Šeruga, D., Fajdiga M., Nagode M. Creep damage calculation for thermo mechanical fatigue. Stroj Vestn-J Mech E 57 371-378 (2011) D0I:10.5545/svime.2010.108.
- [10] Makabe, C., Socie, D.F. Crack growth mechanisms in precracked torsion fatigue specimens. Fatigue Fract Eng Mater Struct 24 607-615 (2001) D0I:10.1046/ j.1460-2695.2001.00430.x.
- [11] Yang, F.P., Kuang, Z.B. Fatigue crack growth for a surface crack in a round bar under multi-axial loading condition. Fatigue Fract Eng Mater Struct 28 963-970 (2005) D0I:10.1111/j.1460-2695.2005.00929.x.
- [12] Tanaka, K., Kato, T., Akinawa, Y. Fatigue crack propagation from a precrack under combined torsional and axial loading. Fatigue Fract Eng Mater Struct 28 73-82 (2005) D0I:10.1111/j.1460-2695.2005.00861.x.
- [13] Grigoriev, N.S., Starkov, K.V., Gorin, A.N., Krajnik, P., Kopač, J. Creep-Feed Grinding: An overview of kinematics, parameters and effects on process efficiency. Stroj Vestn-J Mech E 60 213-220 (2014) D0I:10.5545/sv-jme.2013.1547.
- [14] Nagode, M., Fajdiga, M. Thermo-mechanical modelling of stochastic stress-strain states. Stroj Vestn-J Mech E 52 74-84 (2006).
- [15] Močilnik, V., Gubeljak, N., Predan, J. Time dependent load capacity of the press fit. Tech gasette 19 434-441 (2025) D0I:10.31803/tg-20250115224222.
- [16] EN 10027-1:2016. Designation systems for steels Part 1: Steel names, European Committee For Standardization, Brussels.
- [17] Simulia Abaqus 13.0. Dassault Systems, Vélizy-Villacoublay.
- [18] Wu, D., Li, D., Liu, X., Li, Y., Wang, Y. i Liu, S. Temperature dependence of meso constitutive parameters for advanced high-strength steel. *Trans FAMENA* 48 87-102 (2024) DOI:10.21278/TOF.484063324.
- [19] Stodola, J., Stodola, P. Accelerated Reliability Tests Of Characteristics Of Off-Road Vehicles And Their Parts. Trans FAMENA 48 31-44 (2024) D0I:10.21278/T0F.482049422.

**Acknowledgement** Authors gratefully acknowledges the support of the Slovenian Research and Innovation Agency (ARIS) conducted through the research programme P2-0137 "Numerical and Experimental Analyzis of Mechanical Systems". In addition, this paper has been written to mark the 30th anniversary of the Faculty of Mechanical Engineering and 50th anniversary of the University of Maribor.

Received: 2025-05-26, revised: 2025-07-21, 2025-08-17, Accepted: 2025-08-27 as Original Scientific Paper 1.01.

**Data availability** Data supporting the findings of this study are available from the corresponding author upon reasonable request.

**Author contribution** Vinko Močilnik: Conceptualization, Metodology, Computational Analyzis, Measurements, Validation, Writing – Original Draft; Nenad Gubeljak: Conceptualization, Metodology, Computational Analyzis, Validation, Writing – Review and Editing; Jožef Predan: Conceptualization, Metodology, Computational Analyzis, Validation, Writing – Original Draft.

# Vpliv prednapetja in globokega valjanja na lezenje paličaste torzijske vzmeti

Povzetek Prispevek obravnava obnašanje lezenja torzijskih vzmetnih palic s kombinacijo eksperimentalnega testiranja in numeričnega modeliranja. Eksperimentalne raziskave so bile izvedene na torzijskih vzorcih, ki so bili podvrženi različnim stopnjam prednapenjanja in različnim površinskim obdelavam z globokim valjanjem, pri čemer so se pokazali različni učinki na sproščanje napetosti pri konstantnem kotu zasuka. Simulacije z metodo končnih elementov (MKE), ki vključujejo elasto-visko-plastično obnašanje materiala, so uspešno reproducirale časovno odvisno deformacijo, ki smo izmerili tudi med eksperimentom. Materialni parametri za model MKE so bili izpeljani iz eksperimentalnih podatkov. Ugotovitve kažejo, da dvostopenjski postopek prednastavitve v kombinaciji z vmesnim globokim valjanjem povzroči višje preostale tlačne napetosti v površinskih plasteh v primerjavi z enostopenjskim postopkom prednastavitve. Čeprav je cilj te metode ublažiti lezenje pri konstantnih pogojih obremenitve, ugotavljamo, da je njena učinkovitost omejena. Zmanjšanje deformacij lezenja je opaziti le do stopnje prednastavitve približno 4,3 %; nad tem pragom se deformacije lezenja znatno povečajo in vzmet zgublja na nosilnosti.

**Ključne besede** lezenje, torzijska palica, metoda končnih elementov (MKE), prednapenjanje, globoko valjanje, torzijski moment, kot vzvoja